

High-Speed Electrical Machine with Active Magnetic Bearing System Optimization

Alexander Smirnov¹, Member, IEEE, Nikita Uzhegov², Member, IEEE, Teemu Sillanpää³,
Juha Pyrhönen⁴, Member, IEEE, and Olli Pyrhönen⁵, Member, IEEE

Abstract—High-speed (HS) electrical machines provide high system efficiency, compact design, and low material consumption. Active magnetic bearings (AMBs) bring additional benefits to the HS system, such as elimination of the friction losses, reduced wear and maintenance, and a built-in monitoring system. HS drivetrains are usually designed for specific applications and require a high level of integration. This paper describes a design method of the HS electrical machine supported by AMBs, considering their mutual influence on the system performance. The optimization procedure, which takes into account both the electrical machine and bearing designs, is developed. The optimization is based on a multiobjective genetic algorithm. The selected optimization parameters include the AMB and machine dimensions. The optimization objectives cover the electrical machine performance and the rotordynamics. The results of the proposed optimization algorithm are implemented in the constructed 350-kW, 15 000-r/min induction machine with a solid rotor supported by AMBs. The prototype tests verify the design and optimization results.

Index Terms—AC machine, active magnetic bearings (AMBs), electrical design, high-speed (HS) drive, induction machines, mechanical design, rotating machines.

I. INTRODUCTION

ELECTRICAL machines that operate with high rotational speeds and have a peripheral speed above 100 m/s are referred to as high-speed (HS) electrical machines. An increase in the speed allows us to construct a smaller package, provide a direct connection to the process by eliminating the gearbox,

and improve the system efficiency. Machines of this type are employed in such applications as cutting spindles, flywheel energy storages, gas compressors, air compressors, blowers, and microturbines [1], [2].

With the recent advancement in the power electronics and control technology, active magnetic bearings (AMBs) have become a feasible solution for HS machines. The AMBs levitate the rotor by electromagnetic force, eliminating contact, and, thereby, friction. Thus, without friction, the wear of components is reduced, and there is a less frequent need for maintenance. Other benefits include reduced losses, health monitoring, and lower vibration and noise [3]. Recently, the research has focused on the control aspects of HS machines with AMBs [4]–[6] and the design procedure for the specific bearing type [7]. The bearing design has a significant impact on the overall system, as it strongly affects the rotordynamics.

The design of the HS electrical machine differs in many aspects from conventional machines. Kolondzovski *et al.* [8] have presented the design methodology of high-speed permanent magnet synchronous machines (HS PMSM) and an analysis of the topology limitations. In [9], a design approach for a high-speed induction machine (HSIM) is demonstrated. Again, Uzhegov *et al.* [10] have proposed a multidisciplinary design approach for the HS PMSM with tooth-coil windings. The methodologies incorporate AMBs in the system; however, they do not provide the details of the bearing design. In contrast, the authors in [11] present the AMB design and optimization with limited information about the electrical machine design.

A review of electrical machine optimization (synthesis) methods for permanent magnet machines is presented in [12]. The benchmark study results show the prospects of using a genetic algorithm for the electrical machine optimization problem. The examples of implementing a differential evolution (DE) algorithm involve the design of a 55-kW induction motor for variable-speed applications [13], a 6.7-kW axial flux permanent magnet machine [14], 5.5-kW and 20-MW permanent magnet machines with various topologies [15], and an electrical machine for a pulsatile artificial heart [16]. Methods of finite element (FE) optimization for the PMSM supported by AMBs and software instruments for the optimization are demonstrated in [17] and [18]. None of these examples takes the bearing design into account.

The design of an electrical machine is an iterative process. The iterations are due to the multidisciplinary nature of the system, where thermal, mechanical, and electromagnetic requirements

Manuscript received December 21, 2016; revised March 29, 2017 and May 8, 2017; accepted May 22, 2017. Date of publication June 19, 2017; date of current version October 24, 2017. This work was supported in part by the Department of Chemical and Metallurgical Engineering, Aalto University, and the School of Energy Systems, Lappeenranta University of Technology. (Corresponding author: Alexander Smirnov.)

A. Smirnov was with the Department of Electrical Engineering, School of Energy Systems, Lappeenranta University of Technology, 53850 Lappeenranta, Finland. He is now with the Department of Chemical and Metallurgical Engineering, Aalto University, 16100, Espoo, Finland (e-mail: alexander.smirnov@aalto.fi).

N. Uzhegov was with the Department of Electrical Engineering, School of Energy Systems, Lappeenranta University of Technology, 53850 Lappeenranta, Finland. He is now with Spin Drive, 54100 Lappeenranta, Finland (e-mail: nikita.uzhegov@spindrive.fi).

T. Sillanpää, J. Pyrhönen, and O. Pyrhönen are with the Department of Electrical Engineering, School of Energy Systems, Lappeenranta University of Technology, 53850 Lappeenranta, Finland (e-mail: teemu.sillanpaa@lut.fi; juha.pyrhonen@lut.fi; olli.pyrhonen@lut.fi).

Color versions of one or more of the figures in this paper are available online at <http://ieeexplore.ieee.org>.

Digital Object Identifier 10.1109/TIE.2017.2716875

must be met simultaneously. Each set of requirements is verified by a particular individual or a group of experts who have limited expertise in the rest of the disciplines. This leads to an increased number of iterations and a suboptimal solution. This is of particular importance for HS machines as they operate close to the physical limits. To overcome such an issue, an optimization procedure is applied that takes into account all the knowledge of the experts available and results in a set of solutions lying on the Pareto front. It means that these solutions cannot be improved without sacrificing other criteria. From this set, the expert group selects the desired design point for further verification.

A tailored design is typical in HS drivetrains as it brings additional features and increases the efficiency of the specific application [19], [20]. Therefore, the HS system optimization is of a high value as it can significantly decrease the initial design time and improve the system performance.

This paper describes the steps of a unified design procedure for an HSIM and AMBs. The important parameters affecting the mutual design of the electrical machine and the bearings are presented. A genetic algorithm is implemented to optimize the AMB-HSIM system. Based on the optimization results, a 350-kW 15 000-r/min induction motor with an axially slitted solid rotor, conducting end rings, and AMBs is constructed. The test results show good agreement with the results calculated in the optimization.

The main contribution of this paper is a method of a coupled design and optimization of an HSIM with a solid rotor and AMBs. Even though the proposed optimization procedure is intended for an HSIM with an axially slitted solid rotor and conducting end rings, it can be extended, with slight modifications, to other electrical machine types.

II. DESIGN PROCEDURE

A. Electrical Machine

The general analytical electromagnetic design of the electrical machine under study follows the procedure described in [21]. The design starts with the power and rotational speed required of the machine. An HSIM has a solid rotor, and to improve the electromagnetic performance, axial slits are made in the rotor. Another solution to improve the power factor of the solid rotor machine is the conducting end rings on both sides of the rotor. Fig. 1 shows the rotor structure of the HSIM. The most important output parameters of the electrical machine design include detailed stator and rotor dimensions and materials, machine electromagnetic performance, and losses.

The core losses are calculated separately for the yoke and the teeth based on the average flux density values and the nominal frequency using the Steinmetz equation. The copper losses are calculated based on the winding resistance and the obtained current values. No extra copper losses because of the high frequency were taken into account as the nominal frequency is only 250 Hz. The additional losses were assumed to be 0.5% of the output power. The rotor losses are calculated by the method demonstrated in [22]. The windage losses of the machine active part are calculated based on the procedure presented in [23]. Some of the presented calculation methods cannot ensure

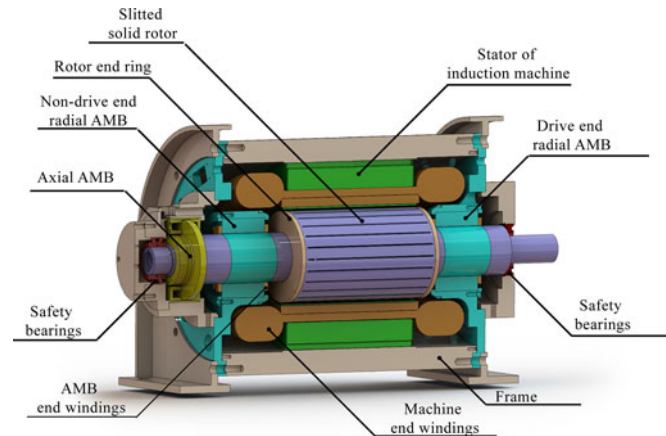


Fig. 1. Model of the system, indicating the locations of the key components.

precise loss calculation; however, the obtained values are suitable for the relative comparison of the various designs.

For the AMB design and rotordynamics analysis, the key machine parameters are the active rotor part structure, dimensions, materials, and the total mass. On the stator side, the end-winding axial protrusion length and the end-winding shape must be defined to locate the AMBs on the rotor.

The initial electrical machine calculation is only the starting point in the AMB-HSIM system design. The AMB design and rotordynamics are of equal importance for the system feasibility and performance. Therefore, the very fundamental electrical machine parameters, such as the rotor outer diameter, can be changed in the iterative AMB-HSIM design process to ensure, for example, undercritical machine operation.

B. Active Magnetic Bearings

The initial point for the bearing design is the force specification that is required to levitate the system with some safety margin. The main aspects and steps of the bearing design are presented in [3]. For HS electrical machines, the homopolar bearing type provides additional benefits such as lower losses and less coupling between the control axes. However, bearings of this type are difficult to manufacture, and their cost is higher [24]. For the system under discussion, a heteropolar bearing was selected. The nominal speed of the rotor is 250 Hz, and it is not a limiting factor for the heteropolar type. Further advantages of this bearing type are associated with its easy and low-cost manufacturing. The particular bearing type is known as an E-core design. This type provides the benefit of splitting the flux in the rotor part between the poles, and the same type avoids the coupling between the neighboring poles of different axes. Consequently, the rotor lamination stack is thinner.

Certain design decisions have been made regarding the bearings. First, the maximum flux density is assumed to be 1.2T, which is defined by the linear region of the material BH curve. Second, the magnetic air gap between the rotor and the stator is fixed to 500 μm , which is a tradeoff between the coil size and the sufficient linear region. Furthermore, the current density in the coils is limited to 5 A/mm^2 at the maximum, as it allows us to

maintain the coil temperature without forced cooling. The final geometry of the bearing with the above-mentioned parameters is defined by the iron ratio. It is the proportion of the length taken by the poles of the total radial circumference at the stator pole shoe.

For the axial bearing, a common C-shape bearing is used. The air gap is $800\ \mu\text{m}$, and the flux density is 0.6T . The function of the increased air gap is to provide some margin in the case of thermal expansion, and the flux density is selected based on the material properties.

For a horizontal system, the forces for radial bearings significantly depend on the rotor mass. Thus, the full rotor structure is evaluated to estimate the requirements set by the total mass. The rotor part of the bearing also contributes to the mass, and therefore, the process is completed in several iterations.

The axial forces do not essentially depend on the rotor mass. In most of the cases, the external forces are significantly higher than the ones from the rotor, and thus, the axial bearing geometry involves only minor changes.

In many cases, the axial bearing, because of the relatively high disc diameter, introduces additional windage losses. For this particular machine, both the required axial forces and the dimensions are small. Fig. 1 shows that the final axial diameter is smaller than the diameter of the electrical machine active part, and the length is significantly smaller. Thus, because of the small forces required, the dimensions and properties of the axial bearing have only a slight impact on the other parameters of the system.

C. Rotordynamics

The rotor dimensions are obtained from the calculations in the above-mentioned design procedures, and the full structure is assembled with certain assumptions.

The first assumption is related to the space occupied by the safety bearings. As the safety bearings can provide a sufficient robustness margin with the rotor mass changes, it is possible to allocate a predefined axial length and rotor diameter to them.

The second assumption is the space required for the sensors. In this machine, eddy current sensors are used. Their geometrical dimensions are quite small, but they should be separated from any external magnetic field to avoid the saturation of the sensor core. Therefore, they should be placed at a certain distance from the magnetic bearings. In this case, the distance of $10\ \text{mm}$ from the bearing end windings has been considered sufficient. The rotor diameter for the sensors was selected to be the same as the outer diameter of the bearing lamination.

The geometrical properties of the interface that connects the rotor to the process, such as an impeller, are well known and do not change for this specific machine.

If the bearing outer diameter is small enough, the bearings can be fitted into the space under the end winding of the electrical machine. In that way, a significant proportion of axial space will be saved. The inner diameter of the end winding is known from the electrical machine calculation, and thus, this information is exploited in the rotor assembly step of the optimization procedure.

The rotor assembly tends to be one of the most geometrically uncertain parts in the whole system. The final geometry is defined by certain aspects of the manufacturing process, and there are many small modifications, which, combined together, can result in significant changes. However, the general idea about the rotordynamics boundaries can be evaluated, but a larger safety margin should be imposed on the corresponding criteria.

For the evaluation of the rotordynamics, an internal finite-element method (FEM) algorithm was used. It implements a Timoshenko beam model according to the method presented by the authors in [25], and it uses MATLAB for computing and providing the results.

A general structure of the system under study is illustrated in Fig. 1. The axial AMB and one of the radial AMBs are located at the nondrive end. The HSIM is in the middle of the frame. The second AMB is at the drive end of the machine. The safety bearings are at the both ends of the rotor. Detailed system parameters are presented in Section IV.

III. OPTIMIZATION

The main objective of the overall optimization procedure is to explore all the possible solutions in the range of the selected parameters. HS electrical machines are operating close to the boundaries of the physical limits [26]. Therefore, small changes in one parameter can significantly expand the safety operating margin. With overall optimization, these relations are identified and applied for performance improvements of the system.

Four parameters were selected as the optimization variables of the system. These parameters have a significant influence on the system electromagnetic performance and rotordynamics. In addition, variation in these variables has a distinct impact on the electromagnetic, mechanical, and rotordynamic performance characteristics of the system.

The first variable is the number of slits in the active part of the rotor. This parameter affects the harmonic content of the air gap flux density, and, thereby, the machine losses. Moreover, it has a direct impact on the rotor structural rigidity and the power factor. The second parameter is the rotor outer diameter. This is the fundamental HS electrical machine parameter because it influences the active part length when the torque and the tangential stress are defined. Simultaneously, the rotor outer diameter significantly affects the amount of losses and the loss distribution in the machine. In addition, the rotor outer diameter defines the rotor peripheral speed and sets requirements on the rotor structural rigidity. The third parameter is the width of the conducting end ring. This parameter influences the rotor inductance, which determines the slip and the power factor. Fig. 2 illustrates the optimization parameters related to the electrical machine rotor.

The last optimization parameter is the iron ratio for the radial bearings. The iron ratio has a significant effect on the axial length taken by the bearing on one side and on the available slot space on the other. Thus, with a higher iron ratio, the axial length is smaller, but the stator outer diameter for the bearings is larger.

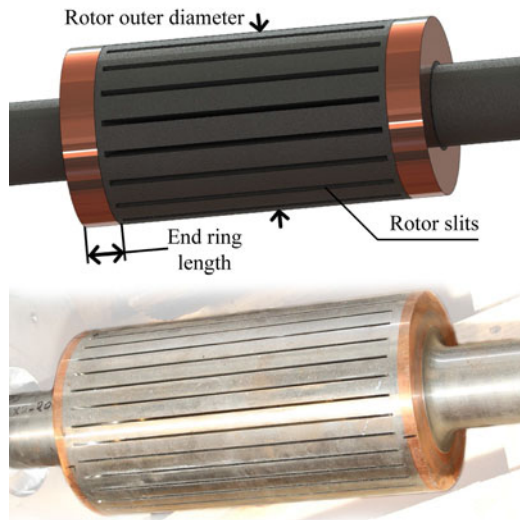


Fig. 2. Model of the rotor with optimization parameters and a photo of the constructed rotor.

TABLE I
PARAMETERS SELECTED FOR THE OPTIMIZATION AND THEIR VARIATION RANGE

Parameter	Minimum value	Maximum value
Number of rotor slits	14	32
Rotor diameter	100 mm	250 mm
End ring width	5 mm	30 mm
Iron ratio for radial bearings	0.3	0.4

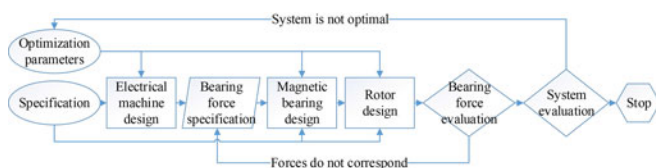


Fig. 3. Optimization scheme.

The parameters of the axial bearings were not included in the optimization procedure because of their insignificant impact on the system, as it was stated in Section II-B. In that way, the number of dimensions for the search space is reduced, thereby saving the computational effort.

The variation range for all parameters was selected based on the engineering experience and data provided in [27] and presented in Table I.

The workflow of the calculation procedure is presented in Fig. 3. The optimization procedure is implemented in MATLAB with Global Optimization Toolbox. The specifications with the fixed parameters of the system along with the optimization parameters are used to design the machine. First, the electrical machine dimensions, electromagnetic performance, losses, and their distribution are calculated. The analytical electromagnetic calculations of the electrical machine are based on the procedure presented in Section II-A. In the next step, the forces required for the bearings are estimated with some margin. The bearing design is calculated according to the procedure described in

	Rotor Slits	Rotor Diameter	Ring Width	Iron Ratio	Rotor Mass	Stator Mass	Losses	Machine Stress	First Flexible	Torque
Rotor Slits	1.000	-0.000	-0.000	-0.000	-0.047	-0.003	0.126	0.000	0.013	0.129
Rotor Diameter	-0.000	1.000	0.000	-0.000	0.693	0.982	-0.859	0.718	0.786	-0.871
Ring Width	-0.000	0.000	1.000	0.000	0.600	0.000	0.005	0.000	-0.436	0.000
Iron Ratio	-0.000	-0.000	0.000	1.000	-0.032	-0.000	0.000	-0.000	0.074	0.000
Rotor Mass	-0.047	0.693	0.600	-0.032	1.000	0.679	-0.614	0.490	0.131	-0.620
Stator Mass	-0.003	0.982	0.000	-0.000	0.679	1.000	-0.757	0.835	0.806	-0.772
Losses	0.126	-0.859	-0.005	0.000	-0.614	-0.757	1.000	-0.292	-0.585	0.999
Machine Stress	0.000	0.718	0.000	-0.000	0.490	0.835	-0.292	1.000	0.692	-0.317
First Flexible	0.013	0.786	-0.436	0.074	0.131	0.806	-0.585	0.692	1.000	-0.601
Torque	0.129	-0.871	0.000	0.000	-0.620	-0.772	0.999	-0.317	-0.601	1.000

Fig. 4. Pearson's linear correlation coefficients for the input and output parameters.

Section II-B, and after that, the full rotor assembly is constructed. With the information about the full rotor mass, the bearing forces are evaluated. If they deviate from the predicted ones, as the second step, the bearing and the rotor assembly are recalculated. This procedure is repeated until a match between the predicted and required forces is found. In most of the cases, this is done in two or three iterations. The final step is the evaluation of the system parameters including the rotordynamics analysis described in Section II-C.

The parameters used to evaluate the system are the mass of the full rotor, the mass of the electrical machine stator part, the total losses, the stress on the rotor because of the rotational speed, the first natural frequency of the rotor, and the shaft torque of the machine at the nominal point.

For the optimization run, the values of the optimization variables are changed based on their previous state and on the results obtained.

As an initial evaluation, a three-level full factorial analysis of the system is performed, resulting in 81 experiments. Based on the obtained result, Pearson's linear correlation coefficients between the selected input and output parameters are estimated. These coefficients are presented in Fig. 4.

It can be seen that the rotor mass is mostly affected by the width of the end rings and the rotor diameter, while the stator mass is mostly dependent on the rotor diameter only. The losses in the system have a strong correlation with the number of slits and the rotor diameter. The rotor stress only depends on the rotor diameter, which is as expected as the stress is defined only for the active part. The frequency of the first flexible mode has a positive correlation with the rotor diameter and negative with the width of the end ring. A thicker rotor makes the system stiffer, while the conducting rings add to the mass and increase the axial length, thereby resulting in a more flexible rotor. There is also a slight positive correlation for the number of slits and the iron ratio. Thus, an increase in the iron ratio makes the rotor shorter. Finally, torque has a positive correlation with the number of slits. The slits intensify the flux penetration into the rotor, and thus, with more slits, it is possible to get more torque.

To sum up, we may conclude that the most influential variable is the Rotor diameter as it has a strong correlation with all output

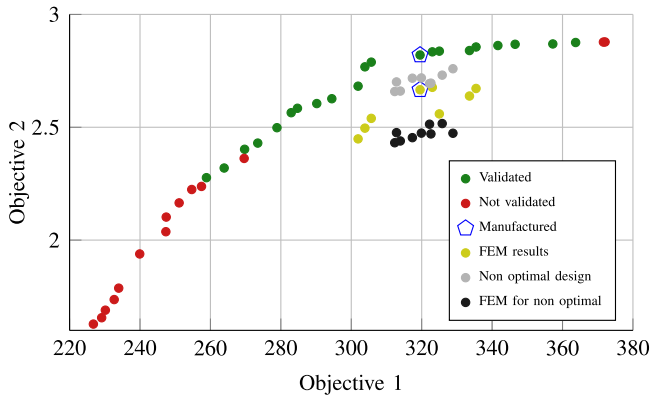


Fig. 5. Pareto front.

parameters. The other variables have less influence on the output parameters; however, their effect is distinct. Therefore, an optimization procedure is required to find the optimum values according to the objectives.

For the optimization procedure, a multiobjective mixed-integer evolutionary algorithm was used. As the objectives, two functions were defined as follows:

$$f_1 = 1.5m_r + m_s, \quad f_2 = \frac{T}{\sqrt{P_{\text{loss}}}} \quad (1)$$

where the rotor and stator masses are denoted by m_r and m_s , respectively. The machine torque is denoted by T , and the losses by P_{loss} . The scaling coefficient of 1.5 is used in the first fitness function based on the correlation value from Fig. 4 between the rotor mass and the stator mass, to make even optimization of both masses. The second function corresponds to “goodness.” It is a measure of average torque production with respect to total losses [12], [15]. The first objective is minimized, while the second objective is maximized as the target is to maximize the torque and minimize the losses.

With the presented modifications, the procedure can also be used for other HS machine and AMB types. For example, in order to use this procedure for the HS PMSM, only certain adjustments are required. First, the analytical submodel of the induction machine should be substituted with the PMSM submodel. Then, as to the optimization parameters, the number of rotor slits and the end ring width should be substituted with parameters that have a high impact on the PM machine performance, such as the PM height and remanence. The algorithm and optimization criteria as well as the submodels for the AMB and rotordynamics can be kept the same.

The population size for the optimization algorithm was selected to be 200 individuals and the number of generations 15. Part of the population in the last generation formed the Pareto optimum front presented in Fig. 5. All solutions on the Pareto front provide an optimal compromise between the two objectives.

The solutions on the Pareto front were also evaluated to satisfy the mechanical constraints. The first constraint invalidates the solutions that do not provide a 50% safety margin for the rotor stress value. The second constraint invalidates the solutions that have the first natural frequency close to the operating range, and, thus, the ones with a frequency below 300 Hz (less than 20%

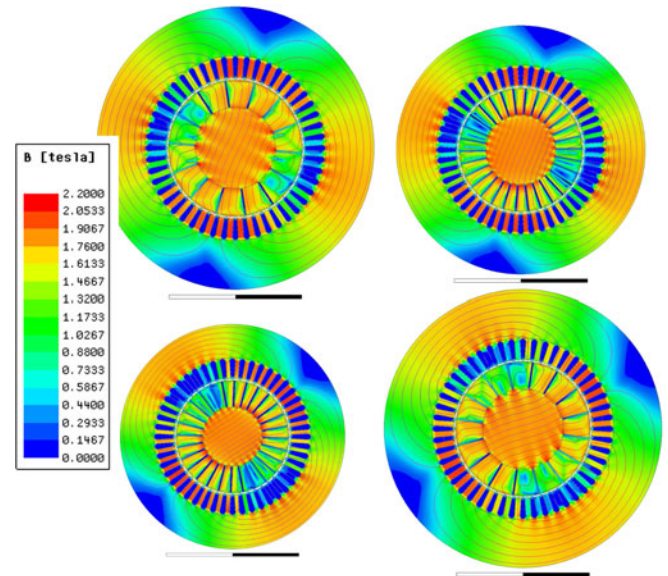


Fig. 6. Examples of four selected machines for FEM verification from the Pareto front. The flux density distribution and the flux lines are shown at the rated operating point.

of the nominal operating point). From the validated solutions, one was selected for a detailed analysis using FE calculations. The system was chosen from the upper right part of the front, meaning that it will have a larger mass and less losses compared with the solutions in the bottom left corner of the front. The selected system after rounding to the manufacturing tolerances has 26 rotor slits, a 195-mm rotor diameter, an end ring length of 10 mm, and bearings with an iron ratio of 0.36. A HSIM prototype with AMBs was constructed based on the optimization and tested to verify the calculation results.

To ensure the accuracy of the analytical solution and the optimization procedure, a set of points from the front near the manufactured system were verified by electromagnetic simulations with the FEM. Additionally, a set of random nonoptimal solutions were generated and selected in the same area for FEM verification. The results are presented in Fig. 5 and selected examples of FEM verification are presented in Fig. 6. It can be seen that the FEM results and the analytical solution agree with each other, and the difference is in the range of 15%. The lower values of the FEM results are explained by the greater losses as the FEM takes into account the local saturation effects.

In addition, based on these simulation results, it has been estimated that on average, the analytical procedure using the same hardware provides results 4000 faster compared with the FEM.

IV. PROTOTYPE MEASUREMENTS

A. Prototype Parameters

Table II shows the key design parameters of the constructed HSIM. The machine has double-layer distributed windings located in 48 stator slots. The winding pitch is selected to be 4/6 to suppress harmonics and to reduce the end-winding axial protrusion length. The main rotor dimensions were selected based

TABLE II
KEY INDUCTION MACHINE PARAMETERS

Parameter	Value
Rated speed, r/min	15 000
Rated power, kW	350
Pole pairs	1
Rated voltage, V	400 (Delta)
Rated current, A	390
Number of stator slots	48
Number of rotor slits	26
Slit width, mm	2.5
Slit height, mm	40
Stack length, mm	300
End ring length, mm	10
Air gap length, mm	2.5
Rotor outer diameter, mm	195
Stator outer diameter, mm	400
Stator core material	M270-50A
Rotor core material	Fe52
End ring material	CuCrZr

TABLE III
KEY PARAMETERS OF MAGNETIC BEARINGS

Parameter	Value
Number of poles	12
Rated voltage, V	210
Rated current, A	12
Stack length, mm	102
Air gap length, μm	500
Rotor outer diameter, mm	106
Stator outer diameter, mm	169
Current stiffness N A^{-1}	219.6
Position stiffness N m^{-1}	2.57×10^6
Lamination material	M270-35A

on the optimization procedure; the rotor structure is shown in Fig. 2. The rotor slit width is 2.5 mm and the rotor slit height is 40 mm. The air gap length is 2.5 mm, which allows us to filter the harmonics and to reduce the rotor losses. The stator core material is M270-50A with a 0.5-mm thickness. This material is selected because the rated point frequency is only 250 Hz. The rotor is made of the ferromagnetic material Fe52 (S355J), and the conducting end rings are made of CuCrZr to tolerate high mechanical stresses.

The bearings were constructed according to the results of the optimization procedure. The material for both the stator and rotor lamination stacks was M270-35A. It is slightly thinner than for the electrical machine to ensure the absence of coupling in the rotor stack. The current and position stiffnesses identified from the prototype are 219.6 N/A and 2.57×10^6 N/m, respectively. The rest of the parameters for the bearings are presented in Table III.

B. Test Installation

Fig. 7 shows a scheme of the equipment connection for the no-load test. The PC provides the main commands to the AMBs and the frequency converter. Information from the machine speed sensor, AMB control and power electronics, temperature sensors, and the frequency converter is monitored on the same

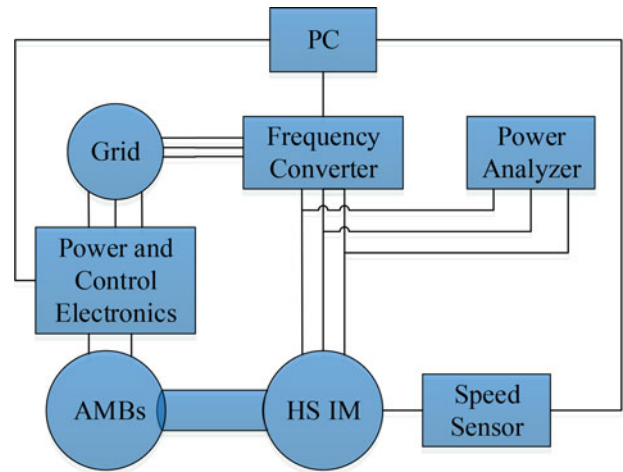


Fig. 7. Equipment connection scheme for the no-load test.

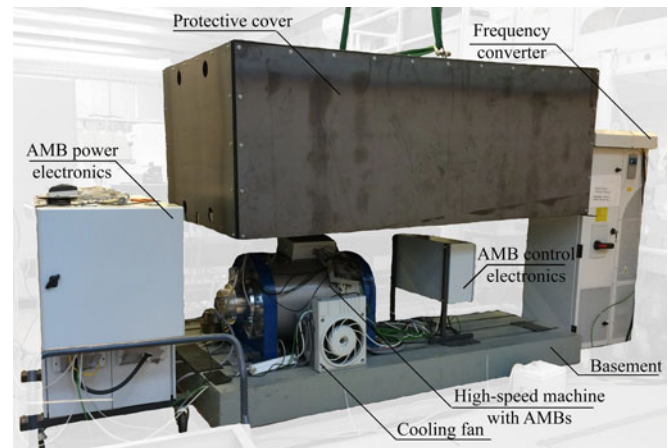


Fig. 8. Test setup.

PC. Power supply from the grid is provided for the frequency converter and the AMB power electronics. A power analyzer Yokogawa PX8000 measures three phases of the electrical machine. Additionally, another power analyzer was used to measure the total AMB power consumption.

Fig. 8 shows a photo of the no-load test setup. The machine is installed and fixed on the base to prevent stator movement and eliminate parasitic vibrations. The AMB power electronics is located in a separate box, and it includes a transformer and frequency converters. The AMB control electronics, which consists of the sensor drivers and the control boards, is located in another box. The electrical machine frequency converter is on the right side in Fig. 8. During the run, the machine is shielded by a protective cover made of rubber and metal sheets for safety reasons as the rotor peripheral speed at 15 000 r/min reaches 153 m/s.

C. Rundown Test

To estimate the windage losses and separate them from the other machine losses, a rundown test was performed. In the test, the rotor is accelerated to the nominal frequency of 250 Hz with an inverter. When the speed is settled, the machine frequency converter is tripped and does not feed the motor. In these

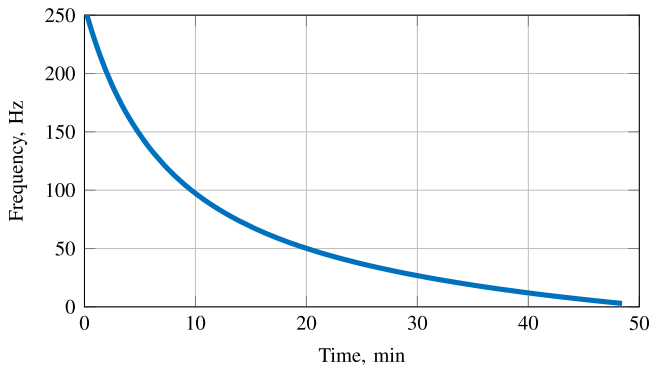


Fig. 9. Rndown measurements.

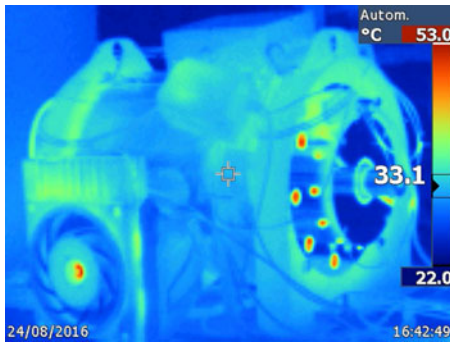


Fig. 10. Thermovisor image of the machine after the no-load test.

conditions, the rotor kinetic energy is slowly dissipated through windage losses and bearing losses. The losses of the AMBs are very small, in the order of a few hundred watts, and most of them are related to the copper losses, which are covered by the AMB power electronics, and only a small fraction of these losses result in a rotor deceleration. Thus, it can be assumed that all the losses are the windage losses caused by the rotor air friction.

In the rundown test, the speed value is recorded every second. Knowing the polar moment of inertia (J_p), windage losses, P_w , are calculated according to the following equation:

$$P_w = \frac{dE_k}{dt} = J_p \omega \frac{d\omega}{dt} + \frac{\omega^2}{2} \frac{dJ_p}{dt} \quad (2)$$

where ω is the rotor angular speed in rad/s, E_k is the kinetic energy [28], and t is the time. The second term in the equation is neglected as the rotor geometric changes are not significant.

The experimental data obtained for the rundown test are presented in Fig. 9. The polar moment of inertia for the rotor is $0.39 \text{ kg}\cdot\text{m}^2$. Using (2) and the rundown test measurements, the windage losses at the nominal speed are estimated to be 2.2 kW .

D. No-Load Test

No-load tests were conducted to verify the performance of both the electrical machine and the AMBs. For this purpose, all measurements were made at the rated rotational speed, which is $15\,000 \text{ r/min}$.

Fig. 10 shows a thermovisor image of the prototype right after the no-load test. It can be seen that the outlet hot air temperature does not exceed $60 \text{ }^\circ\text{C}$. Fig. 11(a) shows the winding

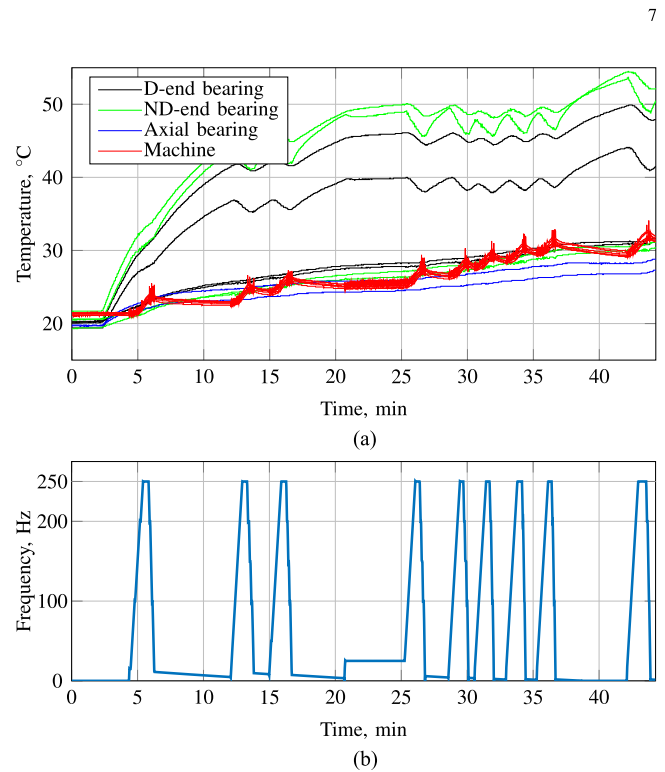


Fig. 11. (a) Temperature distribution in the machine and the AMB windings in the no-load test. Here, the D-end bearing and the ND-end bearing refer to the drive-end and nondrive-end radial bearings, respectively. (b) Rotor frequency profile in the same test.

temperatures of the electrical machine and the AMBs. The measured winding temperatures verify the observation made with the thermovisor.

Fig. 11(b) shows the rotor frequency during the no-load runs. The machine winding temperatures follow the machine runs and idle states. During the acceleration and rotation at the nominal speed, the machine winding temperatures increase. After the deceleration, the machine winding temperatures start to decrease. The behavior of the AMB winding temperature is different; it is significantly less affected by the machine run or idle condition. Because in the idle state the rotor is still levitated by the upper part of the bearings, their temperature is increasing steadily during the test. It can also be seen in Fig. 11(b) that the acceleration to the nominal speed takes only 51.6 s and is limited only by the safety margins of the machine frequency converter. The AMBs can support faster acceleration if the machine frequency controller can provide it.

Table IV shows the results of the no-load test with an array of converter output voltages. All data are presented for the nominal rotational speed. The column “FEM losses” presents the sum of the stator core and rotor eddy-current losses. The next column “FEM and friction losses” takes into account the measured friction losses. The measured losses are compared with the FEM values, which were obtained for three voltage levels. The loss difference is below 7% , which ensures high precision of the model.

TABLE IV
COMPARISON OF NO-LOAD TEST RESULTS AT NOMINAL SPEED

Converter output voltage, V	RMS current, A	FEM losses, W	FEM and friction losses, W	Measured losses, W	Error, %
250	58.4	1360	3560	3388	5.1
260	60.3			3444	
280	64.1			3611	
300	68.1			3733	
320	72.6	1948	4148	3911	6.1
340	76.9			3922	
360	80.8			4144	
380	84.4			4177	
390	86.5	2339	4539	4266	6.4

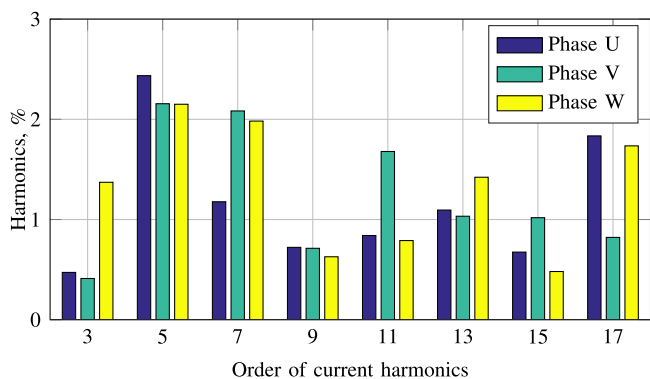


Fig. 12. Measured current harmonics starting from the second harmonic for phase currents. The fundamental harmonics are 119.8, 121.9, and 120.4 A for phases U, V, and W, respectively.

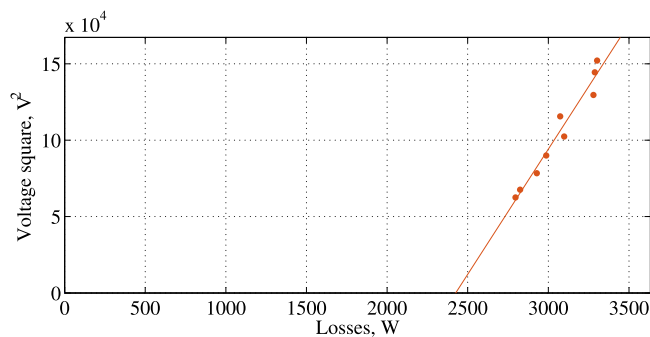


Fig. 13. No-load test hysteresis and windage losses at different voltages and nominal speed. The constant loss component is about 2.4 kW, and it represents the windage losses.

The measured machine losses at no load consist of constant and variable components depending on the voltage level. Fig. 13 shows the losses excluding copper losses versus squared voltage. The copper losses are calculated using the measured winding resistance at the working temperature and eight major current harmonics, which are shown in Fig. 12. Therefore, in Fig. 13, the constant loss component illustrates windage losses, which are independent of the voltage level. The windage losses are equal to 2.4 kW, which corresponds well to the rundown test results. The error is about 8%, and it can be explained by the voltage drop at the motor terminals compared with the converter terminals and by the additional AMB losses at the nominal rotational speed.

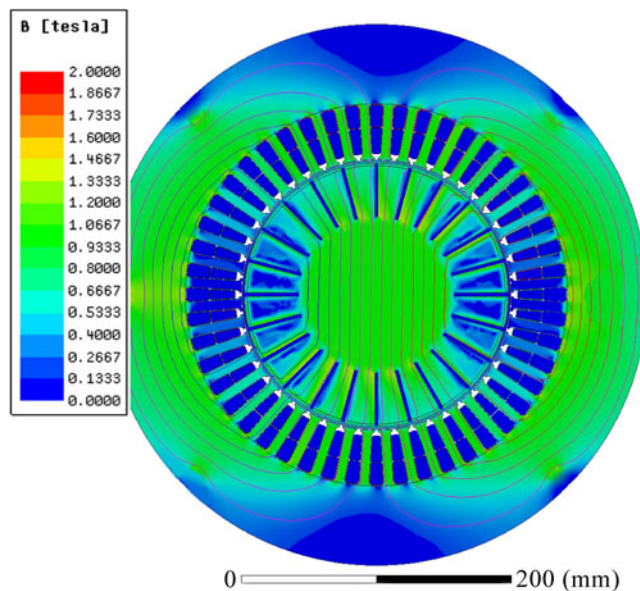


Fig. 14. FEM model of the designed machine with the flux lines and the flux density distribution at no load and rated rotational speed.

The variable loss component in Fig. 13 corresponds to the sum of the stator core and rotor eddy-current losses.

The no-load runs were simulated using the developed 2-D FEM machine model. The measured current harmonics presented in Fig. 12 were used in the model to ensure a high simulation precision. The average total harmonic distortion (THD) for all three phases is 15.4%. The high average THD value is due to the low inductance typical of the HS machine and the absence of filters or chokes between the frequency converter and the machine terminals. A cross section of the designed machine with the flux lines and the flux density distribution in no-load operation at the rated speed and 250-V converter voltage is shown in Fig. 14. The 3-D effects of the solid rotor were taken into account using a method presented in [29]. The simulated stator core losses and rotor losses caused by the eddy current correspond well to the measured data, as shown in Table IV. This verifies the model, simulation, and optimization approach presented in this paper.

V. CONCLUSION

The boundary conditions for the feasibility of the solution were defined through the maximum circumferential stress and the minimum frequency of the first flexible mode of the rotor. A set of variable parameters that have the most impact on the presented objectives were selected. The set comprises the outer diameter of the rotor active part, the number of rotor slits, the width of the conducting end ring, and the iron ratio for radial magnetic bearings. As the objectives for the system optimization, maximization of the torque and minimization of the losses were selected. Furthermore, the total mass minimization was taken as the second optimization objective.

The presented unified design procedure covers both the electrical machine design, the magnetic bearing design, and the rotordynamics of the full rotor assembly. This procedure was

combined with a multiobjective mixed-integer DE optimization algorithm. The objectives were attained by the algorithm through variation of the selected variables. The outcome was a series of optimal solutions lying on the Pareto front.

One solution from the front, based on the engineering experience, was selected for detailed design and verification by the FEA and, then, constructed as a prototype. The prototype machine was tested for magnetic bearing stability up to the nominal speed. The no-load losses at different voltage levels were measured at the nominal speed. The windage losses were estimated by a rundown test. The experimental results demonstrated good agreement with the FEA and the estimations of the unified design procedure.

Thus, it can be concluded that the results of the optimization algorithm and the proposed design procedure were validated by the prototype construction and experimental measurements. The procedure proved to be fast and flexible, and it allows us to evaluate a number of candidate solutions in a fast manner and select the most suitable one.

REFERENCES

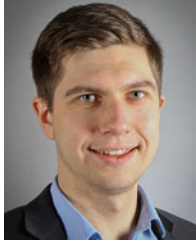
- [1] D. Gerada, A. Mebarki, N. Brown, C. Gerada, A. Cavagnino, and A. Boglietti, "High-speed electrical machines: Technologies, trends, and developments," *IEEE Trans. Ind. Electron.*, vol. 61, no. 6, pp. 2946–2959, Jun. 2014.
- [2] L. Papini, T. Raminosoa, D. Gerada, and C. Gerada, "A high-speed permanent-magnet machine for fault-tolerant drivetrains," *IEEE Trans. Ind. Electron.*, vol. 61, no. 6, pp. 3071–3080, Jun. 2014.
- [3] G. Schweitzer and E. H. Maslen, *Magnetic Bearings*, E. H. Maslen and G. Schweitzer, Eds. Berlin, Germany: Springer, 2009.
- [4] C. Peng, J. Sun, X. Song, and J. Fang, "Frequency varying current harmonics elimination for active magnetic bearing system via multiple resonant controllers," *IEEE Trans. Ind. Electron.*, vol. 64, no. 1, pp. 517–526, Jan. 2017.
- [5] C. Liu, G. Liu, and J. Fang, "Feedback linearization and extended state observer based control for rotor-AMBs system with mismatched uncertainties," *IEEE Trans. Ind. Electron.*, vol. 64, no. 2, pp. 1313–1322, Feb. 2017.
- [6] S. Zheng, Q. Chen, and H. Ren, "Active balancing control of AMB-rotor systems using a phase-shift notch filter connected in parallel mode," *IEEE Trans. Ind. Electron.*, vol. 63, no. 6, pp. 3777–3785, Jun. 2016.
- [7] B. Han, Q. Xu, and Q. Yuan, "Multi-objective optimization of a combined radial-axial magnetic bearing for magnetically suspended compressor," *IEEE Trans. Ind. Electron.*, vol. 63, no. 4, pp. 2284–2293, 2016.
- [8] Z. Kolondzovski, A. Arkkio, J. Larjola, and P. Sallinen, "Power limits of high-speed permanent-magnet electrical machines for compressor applications," *IEEE Trans. Ind. Electron.*, vol. 26, no. 1, pp. 73–82, Mar. 2011.
- [9] C. J. G. Ranft, "Mechanical design and manufacturing of a high speed induction machine rotor," Ph.D. dissertation, North-West Univ., Vanderbijlpark, South Africa, 2010.
- [10] N. Uzhegov, E. Kurvinen, J. Nerg, J. Pyrhönen, J. T. Sapanen, and S. Shirinskii, "Multidisciplinary design process of a 6-slot 2-pole high-speed permanent-magnet synchronous machine," *IEEE Trans. Ind. Electron.*, vol. 63, no. 2, pp. 784–795, Feb. 2016.
- [11] Z. Huang and J. Fang, "Multiphysics design and optimization of high-speed permanent-magnet electrical machines for air blower applications," *IEEE Trans. Ind. Electron.*, vol. 63, no. 5, pp. 2766–2774, May 2016.
- [12] Y. Duan and D. M. Ionel, "A review of recent developments in electrical machine design optimization methods with a permanent-magnet synchronous motor benchmark study," *IEEE Trans. Ind. Electron.*, vol. 49, no. 3, pp. 1268–1275, May 2013.
- [13] A. J. Pina and L. Xu, "A differential evolution algorithm for designing inverter-driven induction motors," in *Proc. IEEE Energy Convers. Congr. Expo.*, Sep. 2014, pp. 279–286.
- [14] X. Yang, D. Patterson, and J. Hudgins, "Design optimization of single-sided axial flux permanent magnet machines by differential evolution," in *Proc. Int. Conf. Elect. Mach.*, Sep. 2014, pp. 1090–1095.
- [15] G. Y. Sizov, P. Zhang, D. M. Ionel, N. A. O. Demerdash, and M. Rosu, "Automated multi-objective design optimization of PM AC machines using computationally efficient FEA and differential evolution," *IEEE Trans. Ind. Electron.*, vol. 49, no. 5, pp. 2086–2096, Sep. 2013.
- [16] A. Pohlmann, M. Leßmann, and K. Hameyer, "Comparative study on optimization methods for a motor-drive of artificial hearts," in *Proc. Int. Conf. Elect. Mach. Syst.*, Oct. 2010, pp. 1754–1758.
- [17] G. Bramerdorfer, A. C. Zavoianu, S. Silber, E. Lughofer, and W. Amrhein, "Possibilities for speeding up the FE-based optimization of electrical machines—A case study," *IEEE Trans. Ind. Electron.*, vol. 52, no. 6, pp. 4668–4677, Nov. 2016.
- [18] D. Reischl *et al.*, "Coupled mechanical and electromagnetic optimization of high speed rotors," in *Proc. 14th Int. Symp. Magn. Bearings*, Linz, Austria, Aug. 2014, pp. 247–250.
- [19] J. Abrahamsson, M. Hedlund, T. Kamf, and H. Bernhoff, "High-speed kinetic energy buffer: Optimization of composite shell and magnetic bearings," *IEEE Trans. Ind. Electron.*, vol. 61, no. 6, pp. 3012–3021, Jun. 2014.
- [20] M. Dems and K. Komeza, "Performance characteristics of a high-speed energy-saving induction motor with an amorphous stator core," *IEEE Trans. Ind. Electron.*, vol. 61, no. 6, pp. 3046–3055, Jun. 2014.
- [21] J. Pyrhönen, T. Jokinen, and V. Hrabovcova, *Design of Rotating Electrical Machines*. Chichester, U.K.: Wiley, 2008.
- [22] K. Boughrara, F. Dubas, and R. Ibtouen, "2-D analytical prediction of eddy currents, circuit model parameters, and steady-state performances in solid rotor induction motors," *IEEE Trans. Magn.*, vol. 50, no. 12, Dec. 2014, Art. no. 7028214.
- [23] J. Saari, "Thermal analysis of high speed induction machine," Ph.D. dissertation, Univ. Helsinki, Helsinki, Finland, 1998.
- [24] A. Filatov and L. Hawkins, "Comparative study of axial/radial magnetic bearing arrangements for turbocompressor applications," *Proc. Inst. Mech. Eng., Part I: J. Sys. Control Eng.*, vol. 230, no. 4, pp. 300–310, Apr. 2016.
- [25] W. J. Chen and E. J. Gunter, *Introduction to Dynamics of Rotor-Bearing Systems*. Victoria, BC, Canada: Trafford, 2005.
- [26] A. Tenconi, S. Vaschetto, and A. Vigliani, "Electrical machines for high-speed applications: Design considerations and tradeoffs," *IEEE Trans. Ind. Electron.*, vol. 61, no. 6, pp. 3022–3029, Jun. 2014.
- [27] J. Hupponen, "High-speed solid-rotor induction machine—Electromagnetic calculation and design," Ph.D. dissertation, Lappeenranta Univ. Technol., Lappeenranta, Finland, 2004.
- [28] M. S. Raymond, M. E. F. Kasarda, and P. E. Allaire, "Windage power loss modeling of a smooth rotor supported by homopolar active magnetic bearings," *J. Tribol.*, vol. 130, no. 2, 2008, Art. no. 021101.
- [29] J. Pyrhönen, J. Nerg, P. Kurronen, and U. Lauber, "High-speed high-output solid-rotor induction-motor technology for gas compression," *IEEE Trans. Ind. Electron.*, vol. 57, no. 1, pp. 272–280, Jan. 2010.



Alexander Smirnov (M'05) received the M.Sc. and D.Sc. degrees in electrical engineering from Lappeenranta University of Technology (LUT), Lappeenranta, Finland, in 2008 and 2012, respectively.

He was a Postdoctoral Researcher with LUT from 2012 to 2016. He is currently a Postdoctoral Researcher with Aalto University, Espoo, Finland. His research mainly concerns high-speed electrical machines and drives, active magnetic bearings, and process control and

optimization.



Nikita Uzhegov (M'14) received the M.Sc. and D.Sc. degrees in electrical engineering from Lappeenranta University of Technology (LUT), Lappeenranta, Finland, in 2012 and 2016, respectively.

He was a Researcher with the School of Energy Systems, LUT, from 2012 to 2016. He is currently a co-Founder and High-Speed Electrical Machine Designer with SpinDrive, Lappeenranta. His research mainly concerns high-speed electrical machines and materials used in electrical machines.



Teemu Sillanpää received the B.Sc. and M.Sc. degrees in electrical engineering in 2012 and 2013, respectively, from Lappeenranta University of Technology, Lappeenranta, Finland, where he is currently working toward the Ph.D. degree with the Control Engineering and Digital Systems Laboratory.

His research interests include power electronic circuits, digital signal processing, and control systems related to active magnetic bearing suspended electrical machines.



Juha Pyrhönen (M'06) was born in Kuusankoski, Finland, in 1957. He received the D.Sc. degree in electrical engineering from Lappeenranta University of Technology (LUT), Lappeenranta, Finland, in 1991.

He became a Professor of electrical machines and drives with LUT in 1997. He is involved in the research and development of electric motors and power-electronic-controlled drives. He has wide experience in the research and development of special electric drives for distributed power production, traction drives, and high-speed applications. Permanent magnet materials and their application in machines play an important role in his research. He is also involved in research on new carbon-based materials for electrical machines.



Olli Pyrhönen (M'14) received the M.Sc. and D.Sc. degrees in electrical engineering from Lappeenranta University of Technology (LUT), Lappeenranta, Finland, in 1990 and 1998, respectively.

Since 2000, he has been a Professor of applied control engineering with LUT. In 2010, he received further teaching and research responsibility in wind power technology with LUT. He has gained industrial experience as an R&D Engineer with ABB Helsinki during 1990–1993 and as a CTO of The Switch during 2007–2010. His current research interests include modeling and control of active magnetic bearings, bearingless machines, renewable power electronics, and electrical drive systems.